Non-Gaussian Random Wave Simulation by Two-Dimensional Fourier Transform and Linear Oscillator Response to Morison Force

Xiang Yuan Zheng[1]
e-mail: xiang.y.zheng@ntnu.no

Torgeir Moan
e-mail: tormo@ntnu.no

Centre for Ships and Ocean Structures,
Norwegian University of Science and Technology,
Trondheim 7491, Norway

Ser Tong Quek
Civil Engineering Department,
National University of Singapore,
Singapore 117576, Singapore
e-mail: cveqst@nus.edu.sg

The one-dimensional fast Fourier transform (FFT) has been applied extensively to simulate Gaussian random wave elevations and water particle kinematics. The actual sea elevations/kinematics exhibit non-Gaussian characteristics that can be represented mathematically by a second-order random wave theory. The elevations/kinematics formulations contain frequency sum and difference terms that usually lead to expensive time-domain dynamic analyses of offshore structural responses. This study aims at a direct and efficient two-dimensional FFT algorithm for simulating the frequency sum terms. For the frequency-difference terms, inverse FFT and forward FFT are implemented, respectively, across the two dimensions of the wave interaction matrix. Given specified wave conditions, the statistics of simulated elevations/kinematics compare well with not only the empirical fits but also the analytical solutions based on a modified eigenvalue/eigenvector approach, while the computational effort of simulation is very economical. In addition, the stochastic analyses in both time domain and frequency domain show that, attributable to the second-order nonlinear wave effects, the near-surface Morison force and induced linear oscillator response are more non-Gaussian than those subjected to Gaussian random waves. [DOI: 10.1115/1.2783888]

Keywords: two-dimensional fast Fourier transform (FFT), wave nonlinearity, Morison force

Introduction

In offshore engineering applications, the random sea surface is usually modeled as a stationary Gaussian process by the linear superposition of harmonic wave components [1]. The water particle kinematics (velocity and acceleration) in fluids follow Gaussian distributions under the linear wave theory. Nevertheless, numerous field observations and laboratory tests have shown that the actual sea elevations tend to exhibit non-Gaussian characteristics. The wave non-Gaussianities are particularly significant in a severe sea state and in shallow water that is a non-negligible factor for the safety considerations of offshore structures. It has been reported by Stansberg [2] that nonlinear wave effects can cause the extreme wave crest heights to increase by as much as 10–20% and the extreme kinematics by about 30%, albeit the energy contribution of the second-order effects to the wave spectrum is small.

The early theoretical descriptions of wave nonlinearity using a second-order correction can be traced to those by Tick [3], Longuet-Higgins [4], and Hasselmann [5]. The successive development of second-order random wave models may be found, to name some, in Sharma and Dean [6], Huang et al. [7], Tayfun [8], and Martinsen and Winterstein [9]. The established models have resulted in many published works on the statistical analysis of the nonlinear random wave elevations, while only limited literatures are available for the kinematics. For this reason, the authors will utilize Langley's [10] convenient eigenvalue/eigenvector approach, however, with some modifications.

To obtain more meaningful statistics of wave force and induced structural response, either time- or frequency-domain stochastic analyses may be applied. Time-domain Monte Carlo simulations are used often because of the relatively less mathematical complexity involved [11]. Owing to the rapid development of computer technology, the Gaussian wave elevation and kinematics that is a single summation of linear wave components can be easily simulated with limited computational time today. It is true even if the summation is performed by a conventional loop considering a large number of frequency components to serve the central limit theorem for a Gaussian realization. The matrix-vector multiplication technique (as well as the dot product of two vectors) embedded in modern computer languages has replaced the performance of time-consuming loops and allows one to save more CPU time [12]. On the other hand, thanks to the efficient fast Fourier transform (FFT) algorithm developed in 1960s, the Gaussian elevation/kinematics may be obtained numerically within a few seconds. The numerical simulation procedures based on one-dimensional inverse transform of Fourier coefficients were presented by Borgman [13] and have been widely applied in offshore engineering.

It appears not that straightforward when dealing with the nonlinear wave simulations. The frequency sum and difference terms that contain double summations over bifrequencies increase the computer work dramatically. This problem becomes more serious when a large number of components are required to capture the reliable higher-order statistics of wave force and structural response [14]. Also, in order to remove sampling uncertainty, dozens or even hundreds of realizations need to be generated [11,15]. In addition, the total wave force on a slender cylinder of an off-

[1]Corresponding author.

Contributed by the Ocean Offshore and Arctic Engineering Division of ASME for publication in the Journal of Offshore Mechanics and Artic Engineering. Manuscript received October 7, 2006; final manuscript received May 2, 2007. Review conducted by Eddie H. H. Shih. Paper presented at the the 25th International Conference on Offshore Mechanics and Arctic Engineering (OMAE2006), Hamburg, Germany, June 4–9, 2006.

shore platform, for instance, demands the integration over local Morison forces at various underwater locations. All these impede the implementation of stochastic analysis through time-domain simulations. Hudspeth and Chen [16] extended the one-dimensional Fourier transform to simulate the non-Gaussian waves by correcting the Fourier coefficients in terms of wave interaction matrices. In reality, such a correction on Fourier coefficients still involves summations over frequencies and costs computer time to some extent. The similar approach, especially designed for the deep-water non-Gaussian wave simulations, was suggested by Stansberg [17]. In the deep-water case, the nonlinear interaction matrix reduces into a much simpler form termed as quadratic transfer function (QTF) [17] that allows the frequency-difference terms to be calculated along the secondary diagonal of the QTF matrix.

For the more general cases of finite water depth, this study adopts two-dimensional fast Fourier transform to simulate the nonlinear portions of not only wave elevation but also kinematics. The numerical efficiency demonstrated is ensured by the FFT algorithm, as revealed by the bi- and trispectral analyses of nonlinear Morison drag effects on an offshore structure [14]. The simulated higher-order statistics of wave elevations are validated by comparing analytical solutions as well as existing empirical fits. Also, the developed two-dimensional FFT technique will be applied to do non-Gaussian realizations of water particle kinematics and associated Morison force. The extended comparative studies will examine the difference between the linear and second-order nonlinear random wave theories when the response time history of a linear oscillator driven by Morison force is computed.

Statistical Analysis of Elevations/Kinematics

In this section, we follow Langley [10] to obtain analytically the cumulants of non-Gaussian wave elevations/kinematics. The originally proposed approach was for wave elevations only but applicable to the water particle velocities as well, while for the water particle accelerations, some necessary modifications are required. Considering the unidirectional wave propagation in a two-dimensional Cartesian plane, the first-order random wave elevation η_1, horizontal water particle velocity u_1, and acceleration a_1 in the water of a finite depth d have the following linear superposition forms [10,13]:

$$\eta_1(x,t) = \sum_{n=1}^{N} (a_n \cos \theta_n + b_n \sin \theta_n) \tag{1}$$

$$u_1(x,z,t) = \sum_{n=1}^{N} R_n(z)(a_n \cos \theta_n + b_n \sin \theta_n) \tag{2}$$

$$a_1(x,z,t) = \sum_{n=1}^{N} \omega_n R_n(z)(- a_n \sin \theta_n + b_n \cos \theta_n) \tag{3}$$

where x is the coordinate for wave propagation direction; z is the vertical coordinate positive upward for measuring the submerged locations below the still water level (SWL); $R_n(z)=\omega_n \cosh k_n(z+d)/\sinh k_n d$ is the linear transfer function for velocity; ω_n is the discrete angular wave frequency and k_n the wave number, computed by the wave dispersion equation $(\omega_n)^2=gk_n \tanh(k_n d)$, with g being the gravity constant and d being the water depth measured from the seabed to the SWL; phase $\theta_n=-k_n x+\omega_n t$; N is number of one-sided harmonic wave components; a_n and b_n are discrete Gaussian random variables if η_1 is assumed to be stationary and Gaussian [10]. These two random variables have the following properties:

$$E[a_n^2] = E[b_n^2] = S_{\eta_1}(\omega_n)\Delta\omega \tag{4}$$

$$E[a_n a_m] = 0 \quad E[b_n b_m] = 0 \quad n \neq m \tag{5}$$

$$E[a_n b_m] = 0 \tag{6}$$

where $S_{\eta_1}(\omega)$ is the specified one-sided wave spectrum for Gaussian waves and $\Delta\omega$ is a discrete frequency interval; $E[\ ]$ is the expectation operator. Assuming that the wave propagation is homogeneous in space, x may be set to be zero for simplicity. Introducing $c_n^2=a_n^2+b_n^2$ and $\varphi_n=\omega_n t+\phi_n$ with $\phi_n=\tan^{-1}(-b_n/a_n)$:

$$\eta_1(t) = \sum_{n=1}^{N} c_n \cos(\varphi_n) \tag{7}$$

$$u_1(z,t) = \sum_{n=1}^{N} R_n(z) c_n \cos(\varphi_n) \tag{8}$$

$$a_1(z,t) = -\sum_{n=1}^{N} \omega_n R_n(z) c_n \sin(\varphi_n) \tag{9}$$

The second-order nonlinear portions of random wave elevations and kinematics are [3–9]

$$\eta_2(t) = \sum_{n=1}^{N}\sum_{m=1}^{N} c_n c_m[v_{nm} \cos(\varphi_n + \varphi_m) + w_{nm} \cos(\varphi_n - \varphi_m)] \tag{7$'$}$$

$$u_2(z,t) = \sum_{n=1}^{N}\sum_{m=1}^{N} c_n c_m[p_{nm} \cos(\varphi_n + \varphi_m) + q_{nm} \cos(\varphi_n - \varphi_m)] \tag{8$'$}$$

$$a_2(z,t) = \sum_{n=1}^{N}\sum_{m=1}^{N} c_n c_m[j_{nm} \sin(\varphi_n + \varphi_m) + l_{nm} \sin(\varphi_n - \varphi_m)] \tag{9$'$}$$

One of the wide-banded models considering the finite water depth d was suggested by Sharma and Dean [6]. In Eqs. (7′), (8′), and (9′), v_{nm}, w_{nm}, p_{nm}, q_{nm}, j_{nm}, and l_{nm} are the nmth entries of respective interaction matrices. They were given as follows:

$$v_{nm} = \frac{1}{4}\left[\frac{D_{nm}^{+} - (k_n k_m - r_n r_m)}{\sqrt{r_n r_m}} + r_n + r_m\right]$$

$$w_{nm} = \frac{1}{4}\left[\frac{D_{nm}^{-} - (k_n k_m + r_n r_m)}{\sqrt{r_n r_m}} + r_n + r_m\right] \tag{10}$$

$$p_{nm} = \frac{g^2 D_{nm}^{+}(k_n + k_m)\cosh k_{nm}^{+}(d+z)}{4\omega_n\omega_m(\omega_n + \omega_m)\cosh k_{nm}^{+}h}$$

$$q_{nm} = \frac{g^2 D_{nm}^{-}(k_n - k_m)\cosh k_{nm}^{-}(d+z)}{4\omega_n\omega_m(\omega_n - \omega_m)\cosh k_{nm}^{-}h} \tag{11}$$

$$j_{nm} = - p_{nm}(\omega_n + \omega_m) \quad l_{nm} = - q_{nm}(\omega_n - \omega_m) \tag{12}$$

where

$$D_{nm}^{\pm}=\frac{(\sqrt{r_n}\pm\sqrt{r_m})[\sqrt{r_m}(k_n^2-r_n^2)\pm\sqrt{r_n}(k_m^2-r_m^2)]+2(\sqrt{r_n}\pm\sqrt{r_m})^2(k_nk_m\mp r_nr_m)}{(\sqrt{r_n}\pm\sqrt{r_m})^2-k_{nm}^{\pm}\tanh k_{nm}^{\pm}d}$$

$$k_{nm}^{\pm}=|k_n\pm k_m| \quad r_n=\omega_n^2/g$$

It can be seen that all interaction matrices are symmetric about n and m except for l_{nm}. For example, $p_{nm}=p_{mn}$ and $l_{nm}=-l_{mn}$. In addition, w_{nm}, q_{nm}, and l_{nm} are zeros if $n=m$. Hence, only the velocity and acceleration are considered. For wave elevations, $R_n(z)$ may be set unity and replace p_{nm} and q_{nm} with v_{nm} and w_{nm}, respectively.

Combine Eqs. (8) and (8′), the total velocity is expressed as

$$u(z,t)=u_1(z,t)+u_2(z,t) \tag{13}$$

that in matrix notation is given by

$$u(z,t)=\mathbf{M}\ \mathbf{x}^T+\mathbf{x}[\mathbf{Q}+\mathbf{P}]\mathbf{x}^T+\mathbf{y}[\mathbf{Q}-\mathbf{P}]\mathbf{y}^T \tag{14}$$

where $\mathbf{P}$ and $\mathbf{Q}$ are symmetric matrices whose nmth entries are $s_ns_mp_{nm}$ and $s_ns_mq_{nm}$; $\mathbf{M}$ is a row vector with the nth element equal to $s_nR_n(z)$, $s_n=\sqrt{S_{\eta_1}(\omega_n)\Delta\omega}$; $\mathbf{x}$ and $\mathbf{y}$ are row vectors with nth entries equal to $x_n=c_n\cos(\varphi_n)/s_n$ and $y_n=c_n\sin(\varphi_n)/s_n$; $\mathbf{x}^T$ is the transpose of $\mathbf{x}$. x_n and y_n are then standard Gaussian variables with the same properties as a_n and b_n. Equation (14) may be reduced to

$$u(z,t)=[\mathbf{M}\ \mathbf{0}][\mathbf{x}\ \mathbf{y}]^T+[\mathbf{x}\ \mathbf{y}][\mathbf{D}][\mathbf{x}\ \mathbf{y}]^T \tag{15}$$

where $\mathbf{0}$ is a one by n zero row vector; $\mathbf{D}$ is the following matrix:

$$\mathbf{D}=\begin{bmatrix}\mathbf{Q}+\mathbf{P} & \mathbf{0}\\ \mathbf{0} & \mathbf{Q}-\mathbf{P}\end{bmatrix} \tag{16}$$

Note that the matrix $\mathbf{D}$ is real and symmetric and consequently its diagonalized form is

$$\mathbf{D}=\mathbf{P_1}\ \mathbf{\Lambda_1}\ \mathbf{P_1}^T \tag{17}$$

where $\mathbf{\Lambda}_1$ is a diagonal matrix of the real eigenvalues λ_n of $\mathbf{D}$, $n=1,2,\ldots,2N$; $\mathbf{P_1}$ is the matrix of which the columns are orthonormal eigenvectors of $\mathbf{D}$, viz., $\mathbf{P_1}\mathbf{P_1}^T=\mathbf{I}$. $\mathbf{I}$ is an identity matrix with dimensions $2N\times 2N$. It follows that u is simply given by

$$u(z,t)=\sum_{n=1}^{2N}\chi_n \tag{18a}$$

$$\chi_n=\beta_nX_n+\lambda_nX_n^2 \tag{18b}$$

where X_n is the nth entry of $[\mathbf{x}\ \mathbf{y}]\mathbf{P_1}$; β_n is the nth entry of the vector-matrix multiplication $[\mathbf{M}\ \mathbf{0}]\mathbf{P_1}$. The orthonormality of eigenvectors results in

$$E[X_n^2]=1 \quad E[X_nX_m]=0 \quad n\neq m \tag{19}$$

such that random variables X_n are standard Gaussian and are mutually independent. It follows that u is the sum of quadratic non-Gaussian variables χ_n, Eq. (18a). The first four cumulants are given as follows [10]:

$$K_1^u=\sum_{n=1}^{2N}\lambda_n \tag{20}$$

$$K_2^u=\sum_{n=1}^{2N}(2\lambda_n^2+\beta_n^2) \tag{21}$$

$$K_3^u=\sum_{n=1}^{2N}(8\lambda_n^3+6\beta_n^2\lambda_n) \tag{22}$$

$$K_4^u=\sum_{n=1}^{2N}48(\lambda_n^4+\beta_n^2\lambda_n^2) \tag{23}$$

The first two cumulants correspond to mean and variance (σ_u^2), respectively. Skewness and kurtosis excess are normalized third- and fourth-order cumulants:

$$\kappa_3^u=K_3^u/\sigma_u^3 \quad \kappa_4^u=K_4^u/\sigma_u^4$$

The kurtosis excess is also defined as kurtosis minus 3. Thus, for a Gaussian random variable, the kurtosis excess is 0. Because the trace of matrix $\mathbf{D}$ is zero, the sum of eigenvalues is also zero and this implies that u has a zero mean (Eq. (20)). It is also noted that the kurtosis excess of velocity is always non-negative.

According to Eqs. (9) and (9′), the total horizontal water particle acceleration is

$$a(z,t)=a_1(z,t)+a_2(z,t) \tag{24}$$

Analogous to u, a can be expressed in matrix notation as

$$a(z,t)=\mathbf{G}\ \mathbf{y}^T+\mathbf{x}[\mathbf{H}+\mathbf{L}]\mathbf{y}^T+\mathbf{y}[\mathbf{H}-\mathbf{L}]\mathbf{x}^T \tag{25}$$

where $\mathbf{H}$ is a symmetric matrix of which the nmth entry is $s_ns_mj_{nm}$, while $\mathbf{L}$ is a skew-symmetric matrix whose nmth entry is $s_ns_ml_{nm}$ and $\mathbf{G}$ is a row vector whose nth element is $-s_n\omega_nR_n(z)$. Different from the cases of u and η, the frequency-difference coefficient matrix $[\mathbf{H}-\mathbf{L}]$ is not symmetric about m and n and the following formulation is thus introduced:

$$a(z,t)=[\mathbf{0}\ \mathbf{G}][\mathbf{x}\ \mathbf{y}]^T+[\mathbf{x}\ \mathbf{y}][\mathbf{A}][\mathbf{x}\ \mathbf{y}]^T \tag{26}$$

where matrix $\mathbf{A}$ is

$$\mathbf{A}=\begin{bmatrix}\mathbf{0} & \mathbf{H}-\mathbf{L}\\ \mathbf{H}+\mathbf{L} & \mathbf{0}\end{bmatrix} \tag{27}$$

where $\mathbf{A}$ is symmetric and has the same property as matrix $\mathbf{D}$. The diagonalization leads to

$$\mathbf{A}=\mathbf{P_2}\ \mathbf{\Lambda_2}\ \mathbf{P_2}^T \tag{28}$$

where matrix $\mathbf{\Lambda_2}$ contains the eigenvalues ε_n of $\mathbf{A}$ ($n=1,2,\ldots,2N$) along its main diagonal and $\mathbf{P_2}$ is the orthonormal eigenvector matrix of $\mathbf{A}$. Similar to u, a is the sum of $2N$ quadratic transformations of independent and standard Gaussian variables:

$$a(z,t)=\sum_{n=1}^{2N}(\iota_nY_n+\varepsilon_nY_n^2) \tag{29}$$

where ι_n is the nth entry of $[\mathbf{0}\ \mathbf{G}]\mathbf{P_2}$; random variable Y_n is the nth entry of $[\mathbf{x}\ \mathbf{y}]\mathbf{P_2}$. Applying Eqs. (20)–(23), the fist four cumulants can be calculated by replacing β_n with ι_n and by replacing λ_n with ε_n. Considering that matrix $\mathbf{A}$ possesses a zero trace, the mean of a is zero as well. In addition, it may be shown that the $2N$ eigenvalues of matrix $\mathbf{A}$ have the property that $\varepsilon_n=-\varepsilon_{2N+1-n}$ and correspondingly $|\iota_n|=|\iota_{2N+1-n}|$ so that the third-order cumulant of a is

$$K_3^a=\sum_{n=1}^{2N}(8\delta_n^3+6\iota_n^2\varepsilon_n)=0 \tag{30}$$

implying that the skewness of horizontal particle acceleration a is identically equal to zero.

The first four cumulants of the kinematics from Eqs. (20)–(23) are useful for the polynomial approximation of the Morison drag force that is necessary for the frequency-domain stochastic analysis of structural responses [18]. The cumulant spectral analysis method has been developed [18] to estimate efficiently the power, bi-, and trispectra and the associated variance, skewness, and kurtosis excess of the total wave force and induced deck displacement for an idealized monopod jack-up platform.

To take into account the varying surface induced inundation effects [19,20] for the structural superharmonic response, the nonlinear portion of kinematics needs further corrections, especially for the zone above the SWL. Several wave stretching/extrapolation methods have been recommended for this problem and a comparative study was conducted for the laboratory measurements of steep waves [21]. On the other hand, without correcting the nonlinear kinematics, the wave inundation effects may also be modeled [18,20] by adding an extra wave load around the SWL to the total force that is integrated from $z=-d$ to the SWL only. In this case, the formulations of kinematics in Eqs. (13)–(24) are valid for $z \leqslant 0$.

Fast Fourier Transform Simulation of Elevation/Kinematics

One-Dimensional Inverse Fast Fourier Transform/Fast Fourier Transform Simulation. In time-domain simulation, the train of linear random wave elevations of overall M number of time steps can be expressed according to Eq. (7) by

$$\eta_1(t_h) = \sum_{n=0}^{N-1} c_n \cos(\omega_n t_h + \phi_n) \quad h = 0,1,\ldots,M-1 \tag{31}$$

where $t_h = h\Delta t$, Δt is a discrete time step. In the deterministic spectral amplitude simulation (Rice [1] and Borgman [13]), c_n is computed as

$$c_n = \sqrt{2S_{\eta_1}(\omega_n)\Delta\omega} \tag{32}$$

and the phase ϕ_n is a sequence of uniformly distributed random numbers in the interval $[0,2\pi)$. Equation (31) may be rewritten as

$$\eta_1(t_h) = \mathrm{Re}\left[\sum_{n=0}^{N-1} (c_n e^{i\phi_n}) e^{i2\pi nh/M}\right] \quad h = 0,1,\ldots,M-1 \tag{33}$$

where i is the imaginary unit and Re[ ] denotes the real part of a complex value inside the square brackets.

While applying the discrete Fourier transform (DFT), M is usually equal to N, a number chosen to be an integer power of 2 for the fast implementation of FFT algorithm. The familiar wave simulation based on the inverse fast Fourier transform (IFFT) is by the following expression [13]:

$$\eta_1(t_h) = \frac{1}{N}\mathrm{Re}\left[\sum_{n=1}^{N} \mathrm{C}_n e^{i2\pi(n-1)(h-1)/N}\right] \quad h = 1,2,\ldots,N \tag{34}$$

where the complex Fourier coefficients are computed as

$$\mathrm{C}_n = N\sqrt{\frac{1}{2}S_{\eta_1}(\omega_n)\Delta\omega}\, e^{i\phi_n} \quad n = 2,\ldots,\frac{N}{2} \tag{35a}$$

$$\text{and } \mathrm{C}_{N+2-n} = \mathrm{C}_n^* \quad n = \frac{N}{2}+2,\ldots,N \tag{35b}$$

where the asterisk "*" denotes complex conjugate. The discrete sequence of wave elevations is then obtained by synthesizing the IFFT of sequence C_n, according to

$$\eta_1(t_h) = \mathrm{IFFT}(C_n) \quad h,n = 1,2,\ldots,N \tag{36}$$

Equation (35a) implies that the two-sided spectrum is invoked and that the Nyquist frequency is at $n=N/2+1$. In other words, if the number of sequence time points is N, the discrete Fourier series representation in the above IFFT procedures involves $N/2$ harmonic components, i.e.,

$$\eta_1(t) = c_0 + \sum_{n=1}^{N/2} c_n \cos(\omega_n t + \phi_n) \tag{37}$$

To decrease Δt or to remove the high-frequency effect, the Fourier coefficients in Eqs. (35a) and (35b) are often padded with trailing zeros. In this case, the number of nonzero-amplitude components will be fewer than $N/2$.

Alternatively, Eq. (33) may be rewritten as

$$\eta_1(t_h) = \mathrm{Re}\left[\sum_{n=0}^{N-1} (c_n e^{-i\phi_n}) e^{-i2\pi nh/N}\right] \quad h = 0,1,\ldots,N-1 \tag{38}$$

that indicates that the sequence of wave elevations is the direct Fourier transform of the following coefficients:

$$C_n = c_n e^{-i\phi_n} = \sqrt{2S_{\eta_1}(\omega_n)\Delta\omega}\, e^{-i\phi_n} \quad n = 0,1,\ldots,N-1 \tag{39}$$

i.e.,

$$\eta_1(t_h) = \mathrm{Re}[\mathrm{FFT}(C_n)] \quad h,n = 0,\ldots,N-1 \tag{40}$$

Different from the IFFT procedures in Eqs. (34)–(37), the one-sided wave spectrum is applied in Eq. (39). Because $\Delta t\Delta f = 1/N$, for the same N and the same cutoff frequency, the frequency resolution Δf of the forward FFT realization in Eq. (40) will be two times finer than that of IFFT in Eq. (36), which in turn makes Δt two times coarser.

To simulate the Gaussian velocity and acceleration, replace the wave spectrum $S_{\eta_1}(\omega)$ by the following velocity and acceleration power spectra, respectively:

$$S_{u_1}(z,\omega_n) = |R_n(z)|^2 S_{\eta_1}(\omega_n)$$

$$S_{a_1}(z,\omega_n) = \omega_n^2 S_{u_1}(z,\omega_n)$$

where $R_n(z)$ is defined following Eq. (3). The sequence of acceleration corresponds to the imaginary part of IFFT/FFT simulation.

Two-Dimensional Fast Fourier Transform Simulation. It can be seen in Eqs. (7′), (8′), and (9′) that the frequency sum and difference terms of the nonlinear random wave elevation and kinematics contain double summations over frequency components. In the following, it will be shown that these double summations can be realized numerically by two-dimensional fast Fourier transforms rather than conventional lengthy loops. First, let us consider the general two-dimensional $M \times N$ forward DFT and inverse DFT pair [22]

$$F(h,r) = \sum_{n=0}^{N-1}\sum_{m=0}^{M-1} f(n,m) e^{-i2\pi nh/N} e^{-i2\pi mr/M} \quad \begin{array}{l} h = 0,\ldots,N-1 \\ r = 0,\ldots,M-1 \end{array} \tag{41}$$

$$f(n,m) = \frac{1}{NM}\sum_{h=0}^{N-1}\sum_{r=0}^{M-1} F(h,r) e^{i2\pi nh/N} e^{i2\pi mr/M} \quad \begin{array}{l} n = 0,\ldots,N-1 \\ m = 0,\ldots,M-1 \end{array} \tag{42}$$

Matrices $F(h,r)$ and $f(n,m)$ are computed by the two-dimensional FFT/IFFT that is denoted as "FFT2" herein

$$F(h,r) = \mathrm{FFT2}[f(n,m)] \quad f(n,m) = \mathrm{IFFT2}[F(h,r)] \tag{43}$$

that is equivalent to calculating separately FFT/IFFT of each dimension of the input matrices [22]:

$$F(h,r) = \mathrm{FFT}_n\{\mathrm{FFT}_m[f(n,m)]\} \tag{44}$$

$$f(n,m) = \mathrm{IFFT}_h\{\mathrm{IFFT}_s[F(h,r)]\} \tag{45}$$

where the RHS of Eq. (44), for instance, indicates that the one-dimensional FFT is performed firstly column by column (m for column) for the input matrix $f(n,m)$, the result of which is then treated by one-dimensional FFT row by row (n for row). Therefore, the FFT subroutine is called for $N\times M$ times. Certainly, the order of n and m can be exchanged without changing the output matrix $F(h,r)$.

The frequency sum term of the nonlinear elevations in Eq. (7′) can be rewritten in the discrete form

$$\eta_2^+(t_h) = \mathrm{Re}\left[\sum_{n=0}^{N-1}\sum_{m=0}^{N-1}(c_n c_m v_{nm} e^{-i\phi_n} e^{-i\phi_m}) e^{-i2\pi nh/N} e^{-i2\pi mh/N}\right] \quad h=0,\ldots,N-1 \tag{46}$$

Compared with Eq. (41), obviously $h=r$. Thus, the vector sequence $\eta_2^+(t_h)$ is exactly the real part of the diagonal entries of the two-dimensional FFT output matrix, namely,

$$F(h,r) = \mathrm{FFT2}[f^+(n,m)] \quad \begin{matrix} h=0,\ldots,N-1 \\ r=0,\ldots,N-1 \end{matrix}$$
$$\eta_2^+(t_h) = \mathrm{Re}[F(h,r)|_{h=r}] \quad h=0,\ldots,N-1 \tag{47}$$

where the frequency sum wave interaction matrix is (Eq. (46))

$$f^+(n,m) = c_n c_m v_{nm} e^{-i\phi_n} e^{-i\phi_m} \quad \begin{matrix} n=0,\ldots,N-1 \\ m=0,\ldots,N-1 \end{matrix} \tag{48}$$

Similarly, the frequency-difference term of elevation is expressible in the following discrete form:

$$\eta_2^-(t_h) = \mathrm{Re}\left[\sum_{n=0}^{N-1}\sum_{m=0}^{N-1}(c_n c_m w_{nm} e^{i\phi_n} e^{-i\phi_m}) e^{i2\pi nh/N} e^{-i2\pi mh/N}\right] \quad h=0,\ldots,N-1 \tag{49}$$

that may be expanded to

$$\eta_2^-(t_h) = \mathrm{Re}\left\{\frac{1}{N}\sum_{n=0}^{N-1}\left[\sum_{m=0}^{N-1}(N c_n c_m w_{nm} e^{i\phi_n} e^{-i\phi_m}) e^{-i2\pi mh/N}\right] e^{i2\pi nh/N}\right\} \quad h=0,\ldots,N-1 \tag{50}$$

Denote the frequency-difference wave interaction matrix as

$$f^-(n,m) = c_n c_m w_{nm} e^{i\phi_n} e^{-i\phi_m} \quad \begin{matrix} n=0,\ldots,N-1 \\ m=0,\ldots,N-1 \end{matrix} \tag{51}$$

then

$$\eta_2^-(t_h) = N\,\mathrm{Re}\left\{\frac{1}{N}\sum_{n=0}^{N-1}\left[\sum_{m=0}^{N-1} f^-(n,m) e^{-i2\pi mh/N}\right] e^{i2\pi nh/N}\right\} \quad h=0,\ldots,N-1 \tag{52}$$

Following Eqs. (44) and (45), we have

$$F(h,r) = \mathrm{IFFT}_n\{\mathrm{FFT}_m[f^-(n,m)]\} \quad \begin{matrix} h=0,\ldots,N-1 \\ r=0,\ldots,N-1 \end{matrix}$$
$$\eta_2^-(t_h) = N\,\mathrm{Re}[F(h,r)|_{h=r}] \quad h=0,\ldots,N-1 \tag{53}$$

where the desired frequency-difference sequence $\eta_2^-(t_h)$ is the real part of the diagonal elements of the two-step FFT/IFFT output matrix times N. Unlike the frequency sum term that may rely on the direct application of available double FFT subroutines, the frequency-difference sequence has be to calculated by computing FFT and IFFT, respectively, across the two dimensions in Eq. (53) with only negligible extra computations.

The above procedures are applicable to simulating nonlinear kinematics as well. The sequence of acceleration corresponds to the imaginary part of the diagonal entries.

Results and Discussions

The procedures developed above are applied to a case that was treated in a previous work [12]. The wave conditions were specified by a JONSWAP wave spectrum with significant wave height H_s=12.9 m, water depth d=75 m, peak wave frequency ω_p =0.417 rad/s, and peak enhancement factor γ=3.3. Based on the second-order random wave model in Eqs. (7′), (8′), and (9′), as many as 180 realizations are generated; each realization corresponds to a storm of 20 min duration. Thus, these realizations can be grouped into sets of 9 to yield 20 sample functions; each sample function is a 3 h storm. The simulations utilize N=2048 and the frequency resolution $\Delta\omega$=0.00511 rad/s. Because nonlinear wave-wave interactions contribute to the high-frequency energy in the measured wave spectrum and the high-frequency energy will induce excessive extreme values of waves, it is important to set a maximum frequency $\omega_{\max}$ for the simulations. Forristall [23] recommended that $\omega_{\max}$ applied for frequency sum calculations be four to five times ω_p, while Stansberg [15] suggested $k_{\max}A_{\mathrm{ext}}<2$; the wave number $k_{\max}$ corresponds to $\omega_{\max}$ and A_{ext} is the expected extreme wave crest for linear random wave theory.

Zhang et al. [24], and Yang and Zhang [25] reported that the second-order nonlinear random theory [3–9] derived based on the conventional perturbation method is applicable to a narrow-banded wave spectrum only and may have a serious divergence problem in calculating water particle kinematics if the bandwidth of wave spectrum is broad. Zhang et al. [24] employed phase modulation method to formulate a hybrid wave model such that the statistics of calculated wave kinematics is not sensitive to $\omega_{\max}$. Here, the peak enhancement factor of JONSWAP spectrum γ=3.3 describes a moderately narrow bandwidth and we have limited wave-wave interactions below the $\omega_{\max}$ value as suggested by Stansberg. Consequently, problems of excessive wave/kinematics extremes and divergences will not appear.

Once the nonlinear random velocity and acceleration are simulated, the Morison force per unit length on a slender member can be computed from

$$f(z,t) = f_I + f_D = C_M A_I a(z,t) + C_D A_D u(z,t)|u(z,t)| \tag{54}$$

where $A_I=\pi\rho(D_{\mathrm{eq}})^2/4$ and $A_D=\rho D_{\mathrm{eq}}/2$; ρ is water density; D_{eq} is the equivalent diameter of the circular member; C_M and C_D are inertia and drag coefficients, respectively. Note that our focus is on the nonlinear random wave effects. The wave-structure interaction effects that can be taken alternatively into account by adjusting the oscillator damping is not included in Eq. (54). Applying the standard time integration procedures, the displacement sequence of the following linear oscillator driven by Morison force is obtained:

$$M\ddot{Y} + C\dot{Y} + KY = f(z,t) \tag{55}$$

The frequency response function of this linear system is

$$H_{Yf}(\omega) = \frac{1}{M(\omega_0^2 - \omega^2 + 2i\xi\omega_0\omega)} \tag{56}$$

where M is the oscillator mass, ω_0 is the free-vibration frequency, and ξ the damping ratio.

The FFT-based computation is so efficient that no more than 10 s is required for simulating an individual sequence of the nonlinear wave elevations. It is much more efficient than the realization using matrix-vector multiplications for the same N and $\Delta\omega$ that needs approximately 50 min. Numerically, the one-dimensional FFT is a process of $O(N\log_2 N)$ multiplications that surpasses the standard double-loop approach, a process of $O(N^2)$ multiplications. Practical computations demonstrate that the difference of computing time in these two processes is even smaller than $(\log_2 N)/N$. Therefore, the two-dimensional FFT scheme proposed for second-order wave/kinematics simulations will further

Table 1 Skewness (κ_3) and kurtosis excess (κ_4) of random wave elevations

	κ_3	κ_4
(a)	0.1892	0.0545
(b)	0.1867	0.0575
(c)	0.1993	0.1191
(d)	0.1972	0.0535
(e)	0.1668	0.0461

Table 2 The mean of extreme wave crests (3 H storms)

	A_{ext}/σ_η (σ_η=3.25 m)
Predicted by Rayleigh distribution, Eq. (59)	3.851
Linear random waves (FFT simulation)	3.480
Nonlinear random waves (2D FFT/IFFT simulation)	4.182
Winterstein's model	4.337
Empirical prediction by Kriebel and Dawson	4.273

outperform the standard triple-loop approach that when taking into account the symmetries of frequency sum and difference terms in Eqs. (7′), (8′), and (9′) is a $O[N^2(1+N/2)]$ computational process.

In Table 1, the higher-order moments of interest, skewness and kurtosis excess, of the non-Gaussian surface elevations are presented. The comparative study includes

(a) the analytical solutions in Eqs. (22) and (23)
(b) the average of the FFT simulations
(c) the parametric model by Vinje and Haver [26] who derived the coefficient of skewness κ_3^η based on second-order Stokes' expansion

$$\kappa_3^\eta = 34.4 H_s/gT_p^2$$

and the coefficient of kurtosis excess in terms of skewness

$$\kappa_4^\eta = 3(\kappa_3^\eta)^2$$

(d) the empirical fit by Winterstein and Jha [27] who made a correction on the kurtosis excess of wave elevations considering the effects of finite water depth d

$$\kappa_4^\eta = \frac{H_s}{L_P}\left(5.45\gamma^{-0.084} + \{\exp[7.41(d/L_p)^{1.22}] - 1\}^{-1}\right) \tag{57}$$

where L_p is the wave length corresponding to T_p; $T_p = 2\pi/\omega_p$
(e) deep-water analytical solutions ($d \to \infty$)

Fits (c) and (d) have been found to agree well with in-field measured data by lasers.

It is worth mentioning that analytical solutions computed by the eigenvalue/eigenvector approach require only a limited number of frequency components (80, say) to yield accurate values of skewness and kurtosis excess.

Table 1 demonstrates that analytically, numerically, and empirically obtained higher-order moments of wave elevations agree well for the intermediate-depth water; see (a)–(d). The kurtosis excess given by Vinje and Haver [26] is almost twice the other three cases because they included the contribution of third-order Stokes' wave effects. By contrast, the deep-water statistics appear smaller, implying the more weakly non-Gaussian waves. Thus, employing deep-water models will underestimate the higher-order statistics of non-Gaussian waves in shallow water. Another important parameter affecting the wave non-Gaussian characteristics is the specified wave height [12].

Table 2 presents the 3 h mean extreme wave crests normalized by the standard deviation (σ_η) of elevations. The analytical σ_η is calculated by Eq. (21). The simulated result is the average of all sample functions. For Gaussian waves, it is known that the largest amplitude approaches closely to Rayleigh distribution and the expected mean extreme of crests is estimated as

$$A_{ext} = \sigma_\eta A_{max} \tag{58}$$

where

$$A_{max} = \sqrt{2\ln N_0}\left(1 + \frac{0.577}{2\ln N_0}\right) \tag{59}$$

where N_0 is the number of wave amplitudes, usually calculated by T/T_z; T is duration of wave storm in seconds and T_z is the zero-crossing period. For the non-Gaussian wave, once its first four moments are analytically computed (Eqs. (20)–(23)), the mean extreme of crests may be estimated applying Winterstein's nonlinear functional transformation [28]:

$$A_{ext} = K\sigma_\eta[A_{max} + h_3(A_{max}^2 - 1) + h_4(A_{max}^3 - 3A_{max})] \tag{60}$$

where K, h_3, and h_4 are polynomial coefficients solved by equating mean, variance, skewness, and kurtosis [28]. The cubic transformation in Eq. (60) is required to be monotonic. Another simple method to empirically predict the mean extreme crest of non-Gaussian waves was proposed by Kriebel and Dawson [29]:

$$A_{ext} = A_{max}(1 + 0.5k_pA_{max}) \tag{61}$$

where k_p is the wave number corresponding to the peak frequency. It can be observed from Table 2 that the simulated mean extremes compare well with the analytical results, though the simulated values appear slightly smaller. The extreme crest predicted by Kriebel and Dawson is rather close to Winterstein's, both of which are around 11.5% higher than the estimation from the Rayleigh distribution. For the effects of wave steepness and sampling variability on the wave extremes, see Stansberg [15].

Figure 1 shows the skewness and kurtosis excess of horizontal water particle velocities $u(z,t)$ as a function of depth z: Analytical solutions versus simulation results. The agreement is seen to be good. The non-Gaussian characteristics of u are significant in the zone near the still water surface and attenuate rapidly with z, due to the exponential functions in wave-wave interaction matrices. As z approaches the sea bottom $z=-d$, the kurtosis excess of the drag term $u|u|$ is fairly close to 8.6667, a value corresponding to case that u is Gaussian. Thus, in Monte Carlo simulations, the linear random wave theory can be employed to calculate the distributed Morison forces near the sea bottom. Note also that the

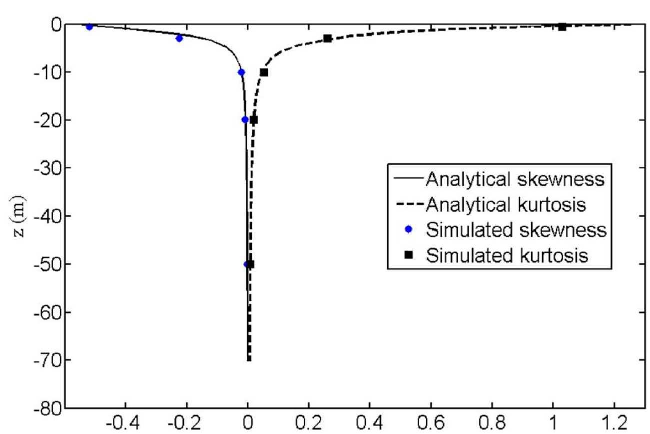

Fig. 1 Skewness and kurtosis excess of velocity attenuate with *z*

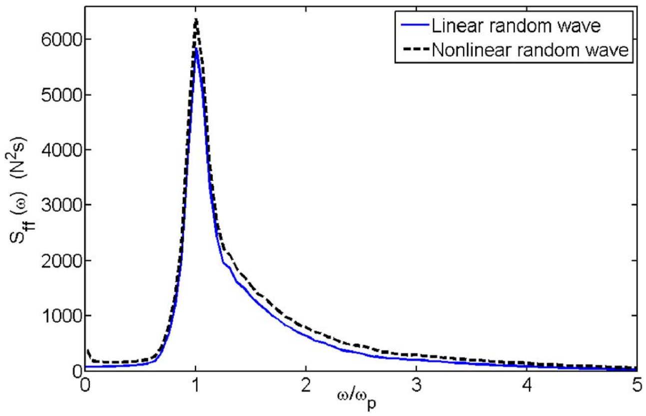

Fig. 2 Power spectrum of Morison force (at z=−3 m)

skewness of surface elevation is positive (Table 1), while the velocity skewness is negative. This has been reported by Hu [30] for the deep-water case. Hence, when the non-Gaussian velocity u is expanded as the cubic polynomials of Gaussian velocity u_1, e.g., Ref. [12],

$$u(z,t) \approx c_0(z) + c_1(z)\frac{u_1(z,t)}{\sigma_{u_1}} + c_2(z)\left[\frac{u_1(z,t)}{\sigma_{u_1}}\right]^2 + c_3(z)\left[\frac{u_1(z,t)}{\sigma_{u_1}}\right]^3 \tag{62}$$

the second-degree polynomial coefficient $c_2(z)$ is negative because of the third-order cumulant of velocity, i.e.,

$$K_3^u = 2c_2[3(c_1+6c_3)^2 + 4c_2^2 + 27c_3^2] \tag{63}$$

It turns out that the skewness of Morison drag term is negative as well and the probability distribution of Morison force tends to be left skewed [12]. Later in Table 4, the induced linear oscillator displacement will be shown to have a negative skewness too.

A jack-up platform (with the natural frequency ω_0 =0.848 rad/s) considered in a previous study [20] is modeled as a linear oscillator. The damping ratio is 0.07 that includes the structural, wave-structure interaction and soil foundation effects. We investigate here the displacement response of the oscillator when driven by a local Morison force 3 m below the SWL. The oscillator mass is assumed to be 1000 kg. The equivalent drag and inertia coefficients used to calculate Morison force are, respectively, 3.25 and 1.60 and the equivalent diameter of platform legs is 1.97 m. Figures 2 and 3, respectively, show the power spectra of force and oscillator displacement. Compared with the linear random wave case, the second-order wave effects result in small

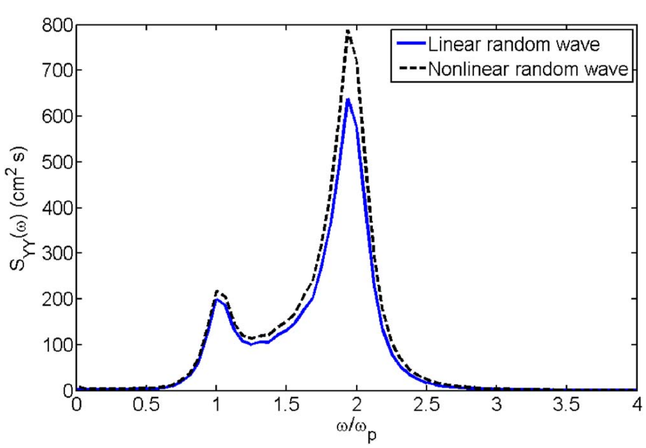

Fig. 3 Power spectrum of oscillator displacement

Table 3 Cumulants of Morison force (z=−3 m)

	Mean (N)	Variance (N^2)	Skewness	Kurtosis excess
(FL)	0	2.0997E+02	0	6.7787
(TL)	7.0709E−03	2.0867E+02	3.5869E−05	6.3222
(FNL)	−6.8290E−01	2.5234E+02	−1.5743	11.8701
(TNL)	−7.0969E−01	2.5059E+02	−1.4994	10.7292

increases for the frequencies higher than ω_p in the force spectrum that in turn, however, causes the oscillator's resonant response at $\omega_0 \approx 2\omega_p$ to be amplified by about 15% (Fig. 3). Without the second-order nonlinear wave effects, the contribution to the resonance at $2\omega_p$ arises from drag nonlinearity only. Therefore, apparently the drag nonlinearity becomes stronger due to the wave nonlinearities. This result can be also supported by looking into the higher-order statistics of both force and oscillator response in Tables 3 and 4.

In the two tables, the first four cumulants (mean, variance, skewness, and kurtosis excess) of four cases are compared:

(A) frequency-domain cumulant spectral analysis. Linear random wave theory (FL)
(B) FFT time simulations. Linear random wave theory (TL)
(C) frequency-domain cumulant spectral analysis. Second-order nonlinear random wave theory (FNL)
(D) FFT/IFFT time simulations. Second-order nonlinear random wave theory (TNL)

The following observations can be made: (1) The simulated results compare well with the frequency-domain solutions, especially for mean and variance values. For kurtosis excess, the frequency-domain analysis produces slightly higher estimations. (2) Due to second-order wave effects, variance increases are remarkable, by around 25% for the force and by around 19% for the oscillator displacement. (3) The force and displacement skewness are no longer zeros, because of the negative velocity skewness aforementioned. (4) For the case of nonlinear random waves, the Morison force exhibits a much stronger non-Gaussian behavior by a significantly higher kurtosis excess. (5) The kurtosis excess of oscillator response gains significant increase too, though this kurtosis excess is much lower than that of wave force due to linear filtering effects. (6) The stronger non-Gaussian behavior of oscillator response for the case of nonlinear random waves can be noticed also by looking into the response mean extremes (Y_{ext}) in the last column of Table 4: Compared to the linear Gaussian wave case, the simulated Y_{ext} is about 15% higher and rather close to the prediction based on the first four moments obtained in the frequency domain and nonlinear transformations (Eqs. (59) and (60)).

Conclusion

Based on second-order nonlinear random wave theories, an analytical method is developed in this study to statistically estimate the cumulants of non-Gaussian wave elevations and kinematics. To solve the time-consuming numerical simulation problem incurred by the double-summation frequency sum and

Table 4 Cumulants and extremes of oscillator displacement

	Mean (cm)	Varianc (cm^2)	Skewness	Kurtosis excess	Y_{ext} (cm)
(FL)	0	21.9136	0	1.8130	28.275
(TL)	2.1091E−03	22.3940	0.0022	1.7302	28.607
(FNL)	−9.4938E−02	26.4359	−0.0843	2.8790	34.222
(TNL)	−9.7044E−02	26.8097	−0.1110	2.5084	32.919

difference terms, an efficient approach applying two-dimensional FFT techniques is proposed. The comparisons conducted demonstrate that the simulated results of wave elevations, including higher-order moments and mean extreme crests, agree well with not only analytical solutions but also empirical fits. The favorable agreement is also observed for horizontal water particle kinematics by comparing the simulated and analytical cumulants. In addition, the stochastic response of a linear oscillator driven by a near-surface Morison force is examined by comparing its power spectra, first four moments, and mean extremes for the cases of linear and nonlinear random waves. Again it is found that both the wave force and the oscillator displacement obtained by simulations compare well with those from a previously developed frequency-domain method [14]. It is pointed out that the nonlinearity of near-surface wave forces is stronger by involving the second-order wave effects and the non-Gaussianity of induced oscillator response is more pronounced than resultant from drag nonlinearity only.

References

[1] Rice, S. O., 1945, "Mathematical Analysis of Random Noise," Bell Syst. Tech. J., **24**, pp. 45–156.

[2] Stansberg, C. T., 1994, "Second-Order Effects in a Random Wave Modeling," *International Symposium: Waves—Physical and Numerical Modeling*, University of British Columbia, Vancouver, Canada, Aug. 21–24, pp. 793–802.

[3] Tick, L. J., 1959, "A Nonlinear Random Model of Gravity Waves (I)," J. Math. Mech., **8**(5), pp. 643–651.

[4] Longuet-Higgins, M. S., 1963, "The Effect of Nonlinearities on Statistical Distributions in the Theory of Sea Waves," J. Fluid Mech., **17**, pp. 459–480.

[5] Hasselmann, K., 1962, "On the Nonlinear Energy Transfer in a Gravity-Wave Spectrum, Part 1, General Theory," J. Fluid Mech., **12**, pp. 481–500.

[6] Sharma, J. N., and Dean, R. G., 1979, "Development and Evaluation of a Procedure for Simulating a Random Directional Second Order Sea Surface and Associated Wave Forces," Ocean Eng. Rep., 20, University of Delaware.

[7] Huang, N. E., Long, S. R., Tung, C. C., and Yuan, Y., 1983, "A Non-Gaussian Statistical Model for Surface Elevation of Nonlinear Random Wave Fields," J. Geophys. Res., **88**(C12), pp. 7597–7606.

[8] Tayfun, M. A., 1986, "On Narrow-Band Representation of Ocean Waves," J. Geophys. Res., **91**(6), pp. 7743–7752.

[9] Martinsen, T., and Winterstein, S. R., 1992, "On the Skewness of Random Surface Waves," *Proceedings of the Second ISOPE Conference* San Francisco, pp. 472–478.

[10] Langley, R. S., 1987, "A Statistical Analysis of Non-Linear Random Waves" Ocean Eng., **14**(5), pp. 389–407.

[11] Bouyssy, V., and Rackwitz, R., 1997, "Polynomial Approximation of Morison Wave Loading," J. Offshore Mech. Arct. Eng., **119**(1), pp. 30–36.

[12] Quek, S. T., Zheng, X. Y., and Moan, T., 2005, "Nonlinear Wave Effects on Distributions of Wave Elevation and Morison Force," *Proceedings of the Ninth ICOSSAR Conference*, G. Augusti, G. I. Schuëller, and M. Ciampoli, eds., Millpress, Rotterdam, pp. 3325–3334.

[13] Borgman, L. E., 1969, "Ocean Wave Simulation for Engineering Design," J. Waterways and Harbors, **95**(4), pp. 557–583.

[14] Zheng, X. Y., and Liaw, C. Y., 2005, "Response Cumulant Spectral Analysis of Linear Oscillators Driven by Morison Forces," Appl. Ocean. Res., **26**(3–4), pp. 154–161.

[15] Stansberg, C. T., 1998, "Non-Gaussian Extremes in Numerically Generated Second-Order Random Waves on Deep Water," *Proceedings of the Eighth ISOPE Conference*, Montreal, Canada, pp. 103–110.

[16] Hudspeth, R. T., and Chen, M. C., 1979, "Digital Simulation of Nonlinear Random Waves," J. Waterways and Harbors, **105**(WW1), pp. 67–85.

[17] Stansberg, C. T., 1993, "Second-order Numerical Reconstruction of Laboratory Generated Random Waves," *OMAE Conference* pp. 143–151.

[18] Zheng, X. Y., and Liaw, C. Y., 2004, "Nonlinear Frequency-Domain Analysis of Jack-Up Platforms," Int. J. Non-Linear Mech., **39**(9), pp. 1519–1534.

[19] Tung, C. C., 1995, "Effects of Free Surface Fluctuation on Total Wave Forces on Cylinder," J. Eng. Mech., **121**(2), pp. 274–280.

[20] Liaw, C. Y., and Zheng, X. Y., 2001, "Inundation Effect of Wave Forces on Jack-Up Platforms," Int. J. Offshore Polar Eng., **11**(2), pp. 87–92.

[21] Stansberg, C. T., and Gudmestad, O. T., 1996, "Nonlinear Random Wave Kinematics Models Verified Against Measurements in Steep Waves," *15th OMAE Conference*, pp. 15–24.

[22] Newland, D. E., 1993, *Random Vibrations, Spectral and Wavelet Analysis*, Longman Scientific & Technical, New York, Chap. 15.

[23] Forristall, G. Z., 2000, "Wave Crest Distributions: Observations and Second-order Theory," J. Phys. Oceanogr., **30**, pp. 1931–1943.

[24] Zhang, J., Chen, L., Ye, M., and Robert, E. R., 1996, "Hybrid Wave Model for Unidirectional Irregular Waves—Part I. Theory and Numerical Scheme," Appl. Ocean. Res., **18**, pp. 77–92.

[25] Yang, J., and Zhang, J., 2000, "Effects of Wave Intermittency and Nonlinearity on Wave Loads," *Proceedings of ETCE/OMAE2000 Joint Conference*, pp. 1–11.

[26] Vinje, T., and Haver, S., 1994, "On the Non-Gaussian Structure of Ocean Waves," *Proceedings of the Seventh BOSS Conference*, 2, MIT, Cambridge, pp. 453–480.

[27] Winterstein, S. R., and Jha, A. K., 1995, "Random Models of Second-order Waves and Local Wave Statistics," *Proceedings of the Tenth ASCE Eng. Mech. Specialty Conference*, pp. 1171–1174.

[28] Winterstein, S. R., 1988, "Nonlinear Vibration Models for Extremes and Fatigue," J. Eng. Mech., **114**, pp. 1772–1790.

[29] Kriebel, D., and Dawson, T. H., 1993, "Nonlinearity in Wave Crest Statistics," *Proceedings of the Second International Symposium on Wave Measurement & Analysis, New Orleans*, LA, pp. 61–75.

[30] Hu, S-L. J., 1993, "Nonlinear Random Water Wave," Book: Computational Stochastic Mechanics, A. H-D. Cheng and C. Y. Yang, eds., Elsevier, New York, pp. 519–543.